A comparison of process damping modelling as local flank face interaction and as macroscopic modal feature in a time domain machining simulation

Grigorii Altshul[a], Mikhail Guskov[*,a], Phillipe Lorong[a]

[a]*PIMM, Arts et Metiers Institute of Technology, CNRS, Cnam, HESAM University, 151 boulevard de l'Hopital, 75013 Paris (France)*

* Corresponding author. Tel.: +33-1-44-24-62-86. *E-mail address:* mikhail.guskov@ensam.eu

Abstract

Dissipative components of tool-workpiece interaction are of major importance in cutting-related vibrations. At the macroscopic vibration scale, such dissipation is usually accounted for by additional generalized damping forces in the equation of motion of the system's elastodynamics. A finer consideration at cutting edge scale would bring up a line-distributed force mostly of ploughing nature. These two scales are usually linked by analytical integration, involving simplifying kinematical assumptions. In the present work a comparative investigation is proposed, for a machining operation, considering both representations in a detailed time domain modeling framework. Tool's cutting edges are represented in a discretized manner, i.e. split into numerous elementary cutters allowing for detailed tool-workpiece interaction force distribution. The matter removal process is modeled via dexel-based surface discretization coupled with finite element-based modal shapes, enabling a consistent machined surface generation representation. Finally, the equations of motion are formulated for modal degrees of freedom and solved by a time marching algorithm. Based on these analyses, the limitations of resulting process damping force terms representations are considered regarding vibrations and interaction force magnitudes.

Peer-review under responsibility of the scientific committee of the 20th CIRP Conference on Modeling of Machining Operations in Mons

Keywords: ploughing; process damping; machining; vibrations

1. Introduction

Since the seminal works by Tobias [1] and Tlusty and Polacek [2], when the link between the flank face tool-workpiece interaction, ploughing and vibration damping phenomena has been considered, this aspect has been investigated in the machining-related vibrations community. Two main approaches consist in considering small vibrations, where the effect of ploughing phenomenon can be linearized into so-called process damping terms, and nonlinear approaches, allowing for considering higher magnitude vibrations. It is the former approach that is in the scope of the present work.

Fundamentally, although the physical aspects of process damping have received numerous physical analyses, such as by Wu [3], or more recently by Theraroz and Oguzhan [4] including plasticity and friction aspects, in practice, direct use of such frameworks is hindered by the difficulty of the direct access to the interaction zone to observe these phenomena in detail. However, on macroscopic scale, these analyses provide basis for the use of more mechanistic definitions, such as considering the kinematic interference volume between the tool's flank face and the workpiece, or global kinematics-to-force constitutive relationships. Thus, the use of process damping coefficient, inversely proportional to the cutting speed, is enabled and can now be found in textbooks [5], especially for constant chip processes, such as turning or drilling.

When it comes to milling, although the time-variable engagement of each tooth adds to the complexity, the previous approach can be adapted. In 2012, Sellmeier and Denkena present a method linking interference volume on a chamfered cutting edge to the local effective clearance angle, then perform the summation over the whole tool in side milling [6]. In 2019, Wöste et al extend this approach to a face milling case [7]. In 2024 [8], Altshul et al develop a similar approach, calculating the effective clearance angle based instant relative velocity of the cutter relative to the workpiece surface.

The goal of this work is to compare this process damping phenomenon, as modeled by the approach from [8], to what

* Corresponding author. Tel.: +33-1-44-24-62-86

2212-8271
Peer-review under responsibility of the scientific committee of the 20th CIRP Conference on Modeling of Machining Operations in Mons
10.1016/j.procir.2025.02.111

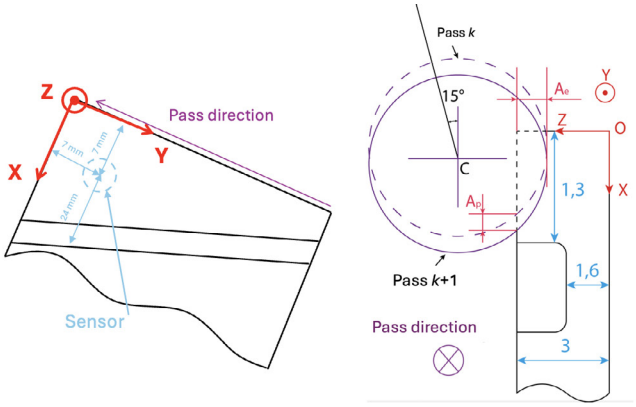

Fig. 1. Milling operation schematic

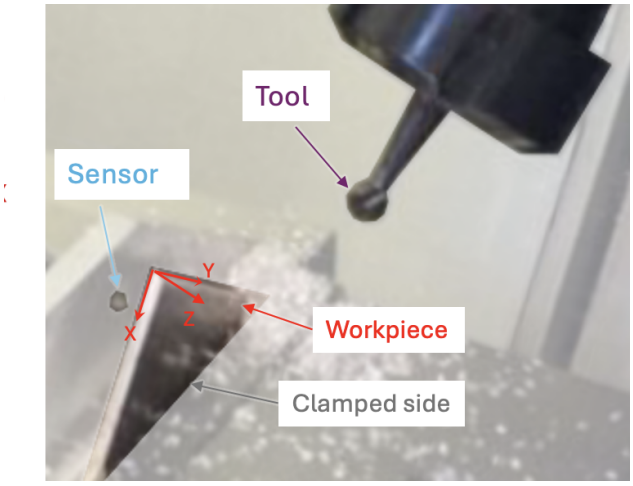

Fig. 2. Experimental setup

could be made by macroscopic damping, as a modification of modal damping acting directly to the dynamical degree of freedom (DOF), on a ball end milling finishing case. The rest of the paper is composed as follows. Section 2 presents the operation under investigation. Section 3 addresses the elastodynamic flexible workpiece with a dexel-based surface modeling, as well as accounting for tool-workpiece interaction. In section 4 simulation results are presented and discussed.

2. Flexible workpiece milling operation

The case study in this article is the climb milling of a triangular titanium alloy plate using a ball end mill. The operation is schematized in figure 1 and the experimental setup is shown on the photo in figure 2. The oblique groove and the tool's direction of travel mean that, as the tool advances, the part becomes increasingly flexible.

During milling tests, plate vibrations were recorded using a Kaman-type inductive sensor (resolution 10^{-4} mm, measurement range 1 mm). The position of the sensor and the test diagram are shown in figure 1. The tool feed direction corresponds to the $-Y$ direction. Milling was carried out in 11 steps. Firstly, 9 roughing steps are made (successive descents in the X direction). These 9 passes are such that the center of the cutter is at $x_c = 0$ (projection of the vector **OC** onto **X**) after the ninth pass. Then, a pass 10 with $a_p = 0.4$ mm and a final pass 11 with $a_p = 0.6$ mm were then performed.

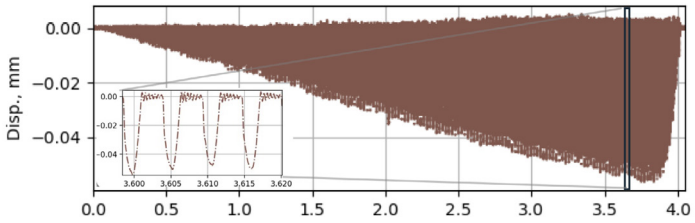

Fig. 3. Displacement under sensor : experimental measurements

For all passes, the feed per tooth is 0.06 mm and the spindle rotation frequency is 2183 rpm. The latter corresponds to a tooth passage frequency of 145.5 Hz. The pass length is 43 mm (approx. 4 seconds). The tool is a ball end mill with a diameter of 8 mm and 4 teeth with a cutting angle varying from $-1°$ to $15°$ along the cutting edge. The clearance angle varies along the cutting edge, but remains close to $7°$ in the cutting zone considered for our operation. The value of the runout is of the order of $3.3 \cdot 10^{-3}$ mm. A 3D scan of the tool was carried out, and the modelling used for the tool during simulations takes account of the measurements, in particular the shape of the teeth.

Figure 3 shows the plot of the displacement measurement during one pass. The signal is composed as a sequence of teeth-induced bumps of increasing magnitude, interceded by out-of-cut time intervals featuring free vibrations of the workpiece. The magnitude evolution is consistent with the distance of the tool from the clamping, with corresponding deformed shape magnitude of the eigenmode of interest, growing quasi-linearly along the tool path.

From the free oscillations of the workpiece between cutting stages, the first three natural frequencies are deduced: 2301 Hz, 8050 Hz and 14200 Hz. The tool is assumed rigid.

3. Modeling framework

The simulation is carried out in nessy2m environment [10]. Globally, the approach consists in a time domain transient simulation of elastodynamics of a machine-tool-workpiece system model during a machining operation. Model inputs include a finite element-like mesh of deformable part with a set of eigenmodes, kinematic description of the operation, geometrical description of cutters with cutting law, and a dexel-based geometry description of the region to be machined. The simulation consists in a Newmark-type time marching and outputs comprise a history of modal coordinates and cutting forces evolution as well as resulting machined surface. Details of application to the present case are described below in this section.

3.1. Workpiece and surface model

Our case study has been designed so that the part is the weak link. This means that the tool is considered rigid, while the part,

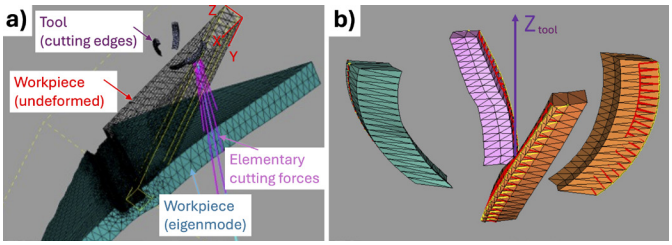

Fig. 4. Model details : a) Workpiece mesh + eigenshape, b) tool active parts (cutting edges + rake faces)

whose finite element mesh is shown in figure 4, is considered flexible. We have chosen to restrict the dynamic model to the part's first mode, with its measured damping rate of 3%. This choice is possible here because the tooth passage frequency is much lower than the part's first natural frequency (factor 16) and, what's more, its first two natural frequencies are very far apart (factor 3.5). The impact of this choice has been assessed, and we have verified by simulation that the addition of further modes has no significant consequences on the results presented below. This is mainly due to the shape of the part, which means that the triangular portion of the part deforms very little and mainly exhibits an oscillating movement around the groove. This creates a flexible "hinge" whose stiffness is directly determined by the depth of the groove.

3.2. *Tool-workpiece interaction modeling*

The material flow around the tool tip is given schematically on the left-hand side of the figure 5, showing two zones: the first is related to chip formation, involving contact between the tool and the workpiece material above point P, and the second to the flow of material under the cutting edge of the tool, linked to the ploughing phenomenon.

In practice, cutting laws are generally predictive models deduced from experimental measurements of cutting forces: using a design of experiment involving tool/material interaction configurations representative of those encountered in practice. These measurements are carried out in the absence of vibration, and the model produced combines chip-forming force and ploughing force.

To dissociate these two effects, we will, as most authors do, decompose the cutting forces into two contributions:

$$\mathbf{F} = \mathbf{F}_{\text{cut}} + \mathbf{F}_{\text{pl}}. \tag{1}$$

Here $\mathbf{F}_{\text{cut}}$ corresponds to cutting forces in the absence of vibration which will come from a model identified from tests previously evoked ($\mathbf{F}_{\text{cut}}$ is mainly associated with the chip formation, and thus with the cutting of the material, but also includes a part coming from ploughing which could be qualified as nominal, *i.e.* in absence of vibrations); and $\mathbf{F}_{\text{pl}}$ can be seen as a disturbance of $\mathbf{F}_{\text{cut}}$ when vibrations appear and modify the orientation of the nominal cutting speed ($\mathbf{F}_{\text{pl}}$ is mainly associated with the ploughing phenomenon).

The right-hand side of the figure shows a schematic representation of the tool's geometric model used in simulation. The cutting face and cutting thickness h used to evaluate $\mathbf{F}_{\text{cut}}$, and the orientation of the flank face $\mathbf{m}$ are shown as well as the speed $\mathbf{V}_i$, which corresponds to the instantaneous speed of the point P of the tool cutting edge relative to the workpiece material. This speed takes into account the spindle's rotational motion, its feed motion and, in our case, the vibrations of the workpiece.

The cutting law was identified so as to reproduce the test as closely as possible (minimization of the gap between cutting forces measurement and simulation).

The form of this law comes from [9]. For each elementary tool, the components of the cutting forces are expressed in an orthonormalized basis noted $(\mathbf{v}, \mathbf{b}, \mathbf{h})$ where $\mathbf{v}$ is directed according to the nominal cutting speed, $\mathbf{h}$ is the unit normal to the local plane tangent to the cutting edge and containing $\mathbf{v}$ ($\mathbf{h}$ is directed from the workpiece material to the tool), $\mathbf{b}$ gives the direct basis. For each component we have :

$$\mathbf{F}_{\text{cut}} \cdot \mathbf{x} = \tilde{b} \, \frac{K_0 \tilde{h} + K \frac{\tilde{h}^2}{h_0}}{1 + \frac{\tilde{h}}{h_0}} \tag{2}$$

with $\mathbf{x} \in \{\mathbf{v}, \mathbf{h}\}$. The component following $\mathbf{b}$ is taken to be zero. The quantities K, K_0, h_0 and n are coefficients of the cutting law (values given in Table 1). Normalized quantities $\tilde{b} = \frac{b}{h_{\text{ref}}}$ and $\tilde{h} = \frac{h}{h_{\text{ref}}}$ represent the width cut and the thickness cut by the elementary tool (calculated at the end of each time increment) and h_{ref} is a normalization length taken to be equal to 10^{-3} m.

	K (N)	K_0 (N)	h_0 (-)
v	875	8750	0.001
h	-525	-22750	0.001

Table 1. Cutting law coefficients

3.3. *Local ploughing force*

Ploughing force is expressed in the plane $(\mathbf{m}, \mathbf{w})$, visible on the right half of figure 5, where $\mathbf{m}$ is the outgoing unit normal of the flank face and $\mathbf{w}$ is a unit vector perpendicular to $\mathbf{m}$ and in the plane containing the instantaneous cutting speed $\mathbf{V}_i$. This ploughing force will thus be broken down into a normal force $\mathbf{F}_{\text{pl}} \cdot \mathbf{m}$ and a sliding force, also called friction force, $\mathbf{F}_{\text{pl}} \cdot \mathbf{w}$.

We therefore propose to define this force, for each elementary tool, in the following form:

$$\mathbf{F}_{\text{pl}} \cdot \mathbf{m} = K_{\text{pl}} \, \tilde{b} \, (\alpha - \alpha_0) \tag{3}$$

$$\mathbf{F}_{\text{pl}} \cdot \mathbf{w} = \mu \, \mathbf{F}_{\text{pl}} \cdot \mathbf{m} \tag{4}$$

where $\tilde{b}$ is the cut width (identical to that used for $\mathbf{F}_{\text{cut}}$), $K_{\text{pl}} = 80$ N/rad, α and α_0 are two clearance angles (visible in figure 5),

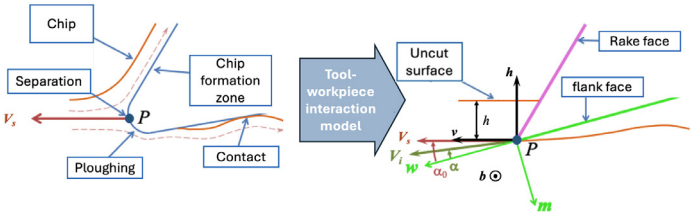

Fig. 5. Material flow around the cutting edge, velocities $\mathbf{V_i}$ and $\mathbf{V_s}$, rake face basis vectors $(\mathbf{v}, \mathbf{b}, \mathbf{h})$, flank face base $(\mathbf{m}, \mathbf{w})$

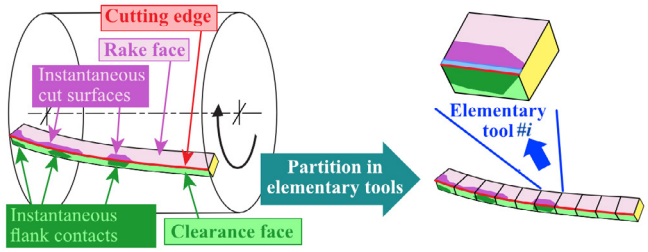

Fig. 6. Cutting edge partition discretisation in nessy2m modeling framework, adapted from [10]

$\mu = 0.1$ is a coefficient of friction. The value of K_{pl}, as shown by Altshul [8] results from updating based on the experimental signal basis.

The angle α is an effective clearance angle that depends on the orientation of $\mathbf{V}_i$ with respect to $\mathbf{w}$, and α_0 is a nominal clearance angle (absence of vibrations) that depends on the orientation of $\mathbf{V}_s$ with respect to $\mathbf{w}$:

$$\alpha_0 = -\arctan\left(\frac{\mathbf{V}_s \cdot \mathbf{m}}{\mathbf{V}_s \cdot \mathbf{w}}\right) \quad \text{and} \quad \alpha = -\arctan\left(\frac{\mathbf{V}_i \cdot \mathbf{m}}{\mathbf{V}_i \cdot \mathbf{w}}\right) \tag{5}$$

where $\mathbf{V}_s$ is the cutting speed in the absence of vibration. In the absence of vibrations, $\alpha = \alpha_0$ implies, with the form chosen in (3), that the force $\mathbf{F}_{\text{pl}}$ is indeed zero.

As the vibration amplitude increases, the effective clearance angle α tends towards zero as the tool approaches the workpiece. This brings us closer to a case of ploughing, which is more akin to a dynamic contact between the part and the tool than to a phenomenon linked to the flow of material under the tool. In such a context, the force applied to the undercut face will increase significantly to avoid any penetration of the workpiece material into the tool.

Figure 6 shows a schematic of integration of an tool edge composed of several elementary tools, including rake face used for the cut swiped volume estimation and flank face.

3.4. Transient simulation

System's dynamics is modelled as a single DOF, based on the workpiece's 1st eigenmode. The equation of motion then reads

$$\ddot{q}_1 + 2\,\zeta_1\,\omega_1\,\dot{q}_1 + \omega_1^2\,q_1 = Q_1 \tag{6}$$

with q_1 the generalized coordinate (modal DOF), $\omega_1 = 14\,458$ rad/s and $\zeta_1 = 0.03$ mode's eigenfrequency and damping ratio, Q_1 generalized force due to the tool–workpiece interaction. This force is composed of two components, in a similar way to the local interaction definition exposed in the precious section:

$$Q_1 = Q_{\text{cut}} + Q_{\text{pl}} \tag{7}$$

with cut and pl indexes standing for cut and ploughing defined as follows. While cutting forces are calculated as modal projection of $\mathbf{F}_{\text{cut}}$:

$$Q_{\text{cut}} = \sum_{i \in C} \boldsymbol{\phi}_1(P_i) \cdot \mathbf{F}_{\text{cut}\,P_i} \tag{8}$$

with C set of elementary tools currently engaged in the cutting process (deep magenta zones on figure 6), P_i reference points of the latter, and $\boldsymbol{\phi}_1(P_i)$ mass-normalized deformed shape magnitude in those points; the ploughing forces are accounted for in two ways:

- either based on a local condition of each elementary cutter, *i.e.* similarly to (8):

$$Q_{\text{pl}}^{(1)} = \sum_{i \in C} \boldsymbol{\phi}_1(P_i) \cdot \mathbf{F}_{\text{pl}\,P_i} \tag{9}$$

  which is as accurate as the Q_{cut} evaluation, but also just as costly,
- or in a macroscopic perspective, as a contribution to the damping of the modal oscillator q_1

$$Q_{\text{pl}}^{(2)} = -2\,\zeta_{\text{pl}}\,\omega_1\,\dot{q}_1\,H(|Q_{\text{cut}}|) \tag{10}$$

  with H Heaviside step function and ζ_{pl} apparent contribution of the process damping to the modal damping. This second option amounts to considering the system's response globally.
  In the second case, relevant value for ζ_{pl} is not known *a priori* and will be subject to analysis by the following.

Finally, the simulation is carried out on the equation (6) is solved by central difference time marching.

4. Simulation results and discussion

Figure 7 shows all the resulting displacement signals in the sensor location for the following cases : local damping model ($K_{\text{pl}} = 80$ N/rad), macro damping model for several test values of $\zeta_{\text{pl}} \in \{0.03, 0.10, 0.30, 0.90\}$, overlayed with experimen-

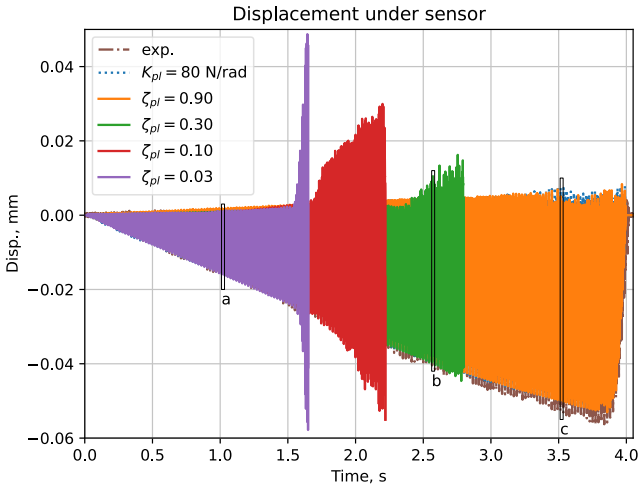

Fig. 7. Displacement under sensor : experimental measurements and simulation results

tal measurements. The set of values for ζ_{pl} was built as a logarithmic scan, increasing at each step by a factor ≈ 3, starting from the damping of the workpiece.

In the beginning ($t < 1.5$ s) all the waveforms follow the shape of the experimental signal, but then several simulated cases exhibit notable non realistic oscillation increase followed by a crash. A crash mainly corresponds to excessive velocities resulting in nonphysical cut volumes. Namely, $\zeta_{\text{pl}} = 0.03$ crashes at $t = 1.65$ s, $\zeta_{\text{pl}} = 0.10$ at $t = 2.22$ s and $\zeta_{\text{pl}} = 0.30$ at $t = 2.80$ s. Only the cases $Q_{\text{pl}}^{(1)}$ (with $K_{\text{pl}} = 80$ N/rad) and $Q_{\text{pl}}^{(2)}$ (with $\zeta_{\text{pl}} = 0.90$) went through the entire pass simulation.

To see in detail the responses at different stages of the pass, zoomed views corresponding to boxes (a, b, c) are shown on figures 8 and 9. We can notice on (a) that at low magnitudes, the cases with smaller ζ_{pl} (0.03 and 0.10) follow the best the experimental signal. In the interval between instants (a) and (b) these cases become divergent though, as mentioned previously. The local damping model-based response (dotted blue) is superimposed on the lowest macroscopic damping case (violet).

In (b) we see that the green line follows close to the experimental data, in the beginning of each tooth bite, but that every time in the second half of tooth engagement the macroscopic damping (ζ_{pl}) fails to suppress unrealistic oscillations, resulting in strong free vibrations just afterwards, which are not decayed sufficiently before the next tooth comes into cut. As can be observed on figure 9, this stage corresponds to the increasing divergence of the green line ($\zeta_{\text{pl}} = 0.30$) undergoing a scenario similar to the two other crashes. As may be seen on figure 9(b), the local damping model-based response in this plot follows closely the macroscopic damping case $\zeta_{\text{pl}} = 0.3$ (green) during the entry stage ($2.5637 \text{ s} < t < 2.5647$ s), while during the exit stage ($2.5650 \text{ s} < t < 2.5660$ s) the latter case features increasing excessive vibrations.

The last zoom (c) shows a high magnitude response in which the two remaining simulated signals are closer to one another than to the experimental data, which they are still quite close to.

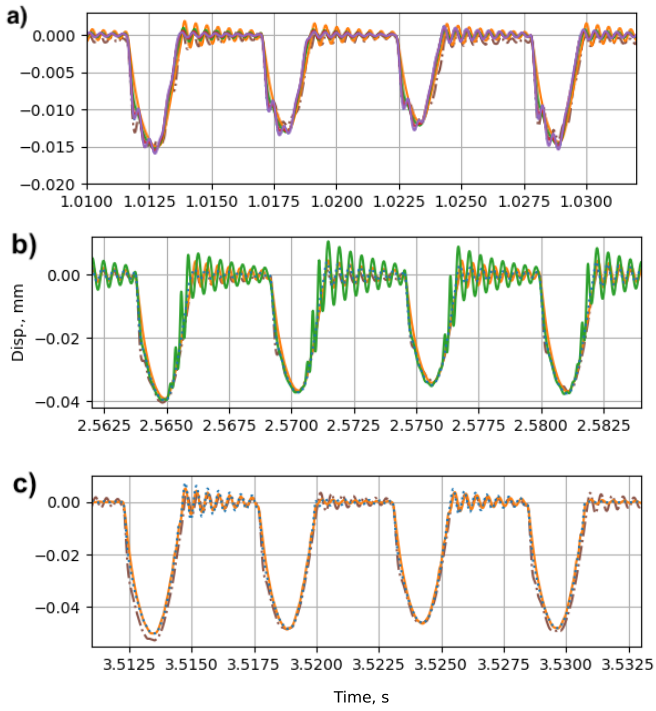

Fig. 8. Displacement under sensor : experimental measurements and simulation results, zoom on one tool rotation period at a) 1.01s, b) 2.56 s, c) 3.51 s. Color legend identical to that of figure 7

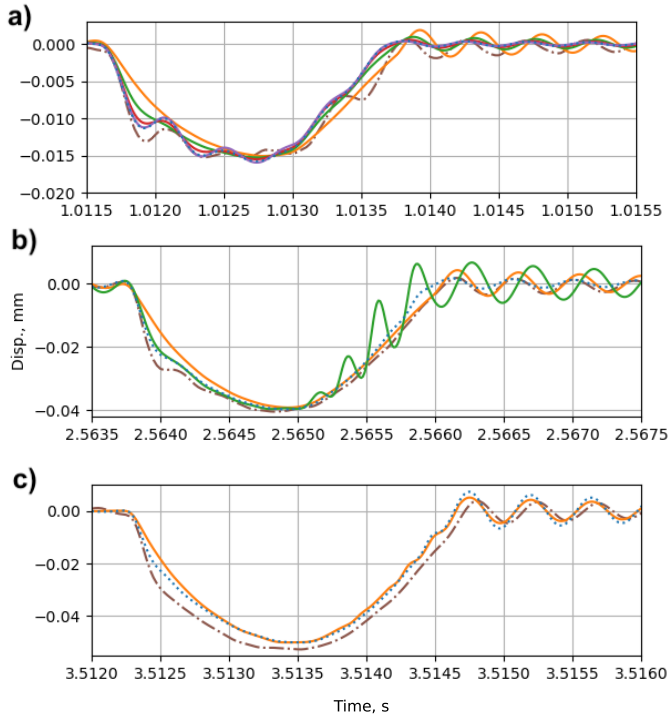

Fig. 9. Displacement under sensor : experimental measurements and simulation results, zoom on one tooth action at a) 1.01s, b) 2.56 s, c) 3.51 s. Color legend identical to that of figure 7

They feature some visible spread though at the no-cut part. The differentiation per tooth visible on figure 8 might suggest some unevenness in teeth cutting or ploughing properties. When focusing on the comparison simulation-issued and measured signals, although the shape and scale of the waveforms are mainly similar, one can notice that some differences that can be summarized as excessive apparent damping during the entry stage (left slope of bumps corresponding to one tooth work) and underestimation at the exit stage (right slope respectively), as can be seen on figure 9. These differences can be interpreted as suggesting that the models used, based on linear relationships (3) and (10), might be too simplistic to reflect such level of detail.

To summarize, the macroscopic description for ploughing (10) enables to follow the response provided detailed local model for ploughing terms (9), with apparent ζ_{pl} steadily increasing throughout the operation. This increase starts from the level of the workpiece modal damping (at $t \approx 0$, representative ζ_{pl} is comparable to ζ_1), and then exceeds it by above one order of magnitude (at $t > 3$ s $\zeta_{\text{pl}} > 0.30$).

In terms of computational cost, although the macroscopic approach is numerically only slightly less costly than the local one (respectively, 862 s vs 894 s simulation run time[1]), it can be considerably more practical because easier to define. Indeed, if the general response magnitudes are of interest, they are well represented by the case $\zeta_{\text{pl}} = 0.9$ which is an overestimation during most of the time.

5. Conclusion

Two approaches to accounting for ploughing are applied to a ball-end milling finishing operation of a flexible part are compared. The first approach based on a finer, local definition of ploughing forces, and the second one, considering a macroscopic description of ploughing as a contribution to modal damping. While the former allows for the closer and more robust representation of experimentally observed data, the latter, very easily defined, enables a global outlook on the ploughing action on the system's dynamics. Thus, the process damping, which is naturally better accounted for by a definition bound to the tool location, can be represented by a simple modal damping force with a constant coefficient as long as one seeks to simply represent magnitude and a general shape of the response waveform.

In the flexible workpiece milling operation considered, it is notable that additional damping due to the machining process is necessary to the model so as to simulate system's response without undergoing excessive vibrations. Macroscopic eigenmode-wise representation has shown that although an overestimated constant modal damping model enables generally realistic vibration magnitudes, effective level of this process damping term is subject to strong variation, from 1 to up to 10+ times above the system's intrinsic damping.

[1] tested on a MacBook Pro computer, M1 Max processor, 64 GB RAM

References

[1] Tobias, S. A. "The Vibrations of Vertical Milling Machines under Test and Working Conditions." Proceedings of the Institution of Mechanical Engineers 173, no. 1 (June 1, 1959): 474–510. https://doi.org/10.1243/PIME_PROC_1959_173_047_02.

[2] Tlusty, J., and M. Polacek. "The Stability of Machine Tools against Self Excited Vibrations in Machining." In Proceedings of the ASME International Research in Production Engineering, Pittsburgh, USA, 465:474, 1963.

[3] Wu, D. William. "A New Approach of Formulating the Transfer Function for Dynamic Cutting Processes." Journal of Manufacturing Science and Engineering 111, no. 1 (1989): 37–47.

[4] Theraroz, Jonathan, and Oguzhan Tuysuz. "A Generalized Machining Process Damping Model for Orthogonal Cutting." Journal of Manufacturing Science and Engineering (2024): 1-40.

[5] Altintas, Yusuf. Manufacturing Automation: Metal Cutting Mechanics, Machine Tool Vibrations, and CNC Design. Cambridge University Press, 2012.

[6] Sellmeier, V., and B. Denkena. "High Speed Process Damping in Milling." CIRP Journal of Manufacturing Science and Technology 5, no. 1 (January 1, 2012): 8–19. https://doi.org/10.1016/j.cirpj.2011.12.001.

[7] Wöste, F., J. Baumann, P. Wiederkehr, and T. Surmann. "Analysis and Simulation of Process Damping in HPC Milling." Production Engineering 13, no. 5 (October 1, 2019): 607–16. https://doi.org/10.1007/s11740-019-00912-4.

[8] Altshul, Grigorii, Philippe Lorong, Mikhail Guskov, Amran Lounès Illoul, Théo Dorlin, And Habib Karaouni. "Modélisation des efforts en dépouille lors de l'usinage de voiles minces en titane." Grenoble, France, 2024.

[9] Paris, H., D. Brissaud, and A. Gouskov. "A More Realistic Cutting Force Model at Uncut Chip Thickness Close to Zero." CIRP Annals 56, no. 1 (2007): 415–18. https://doi.org/10.1016/j.cirp.2007.05.096.

[10] Coffignal, Gérard and Lorong, Philippe and Illoul, Lounès. "A general method to accurately simulate material removal in virtual machining of flexible workpieces" (2015), https://hal.science/hal-03184509/document